This article was downloaded by:
On: *22 January 2011*
Access details: *Access Details: Free Access*
Publisher *Taylor & Francis*
Informa Ltd Registered in England and Wales Registered Number: 1072954 Registered office: Mortimer House, 37-41 Mortimer Street, London W1T 3JH, UK

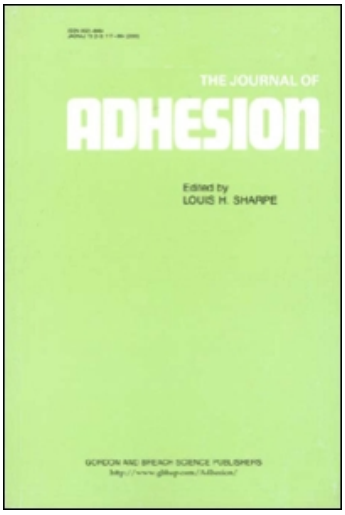

The Journal of Adhesion
Publication details, including instructions for authors and subscription information:
http://www.informaworld.com/smpp/title~content=t713453635

Cohesive Zone Models of Polyimide/Aluminum Interphases

K. M. Liecht; A. Shirani[a]; R. G. Dillingham[b]; F. J. Boerio[b]; S. M. Weaver[b]
[a] Mechanics of Solids, Structures and Materials, The University of Texas at Austin, Austin, Texas, USA
[b] Department of Materials Science and Engineering, The University of Cincinnati, Cleveland, OH, USA

To cite this Article Liecht, K. M. , Shirani, A. , Dillingham, R. G. , Boerio, F. J. and Weaver, S. M.(2000) 'Cohesive Zone Models of Polyimide/Aluminum Interphases', The Journal of Adhesion, 73: 2, 259 — 297
To link to this Article: DOI: 10.1080/00218460008029309
URL: http://dx.doi.org/10.1080/00218460008029309

PLEASE SCROLL DOWN FOR ARTICLE

Full terms and conditions of use: http://www.informaworld.com/terms-and-conditions-of-access.pdf

This article may be used for research, teaching and private study purposes. Any substantial or systematic reproduction, re-distribution, re-selling, loan or sub-licensing, systematic supply or distribution in any form to anyone is expressly forbidden.

The publisher does not give any warranty express or implied or make any representation that the contents will be complete or accurate or up to date. The accuracy of any instructions, formulae and drug doses should be independently verified with primary sources. The publisher shall not be liable for any loss, actions, claims, proceedings, demand or costs or damages whatsoever or howsoever caused arising directly or indirectly in connection with or arising out of the use of this material.

J. Adhesion, 2000, Vol. 73, pp. 259–297
Reprints available directly from the publisher
Photocopying permitted by license only

© 2000 OPA (Overseas Publishers Association) N.V.
Published by license under
the Gordon and Breach Science
Publishers imprint.
Printed in Malaysia.

Cohesive Zone Models of Polyimide/Aluminum Interphases*

K. M. LIECHTI [a,†], A. SHIRANI [a], R. G. DILLINGHAM [b], F. J. BOERIO [b] and S. M. WEAVER [b]

[a]*Research Center: Mechanics of Solids, Structures and Materials, The University of Texas at Austin, Austin, Texas 78712-1085, USA;*
[b]*Department of Materials Science and Engineering, The University of Cincinnati, Cleveland, OH 45221-0012, USA*

(Received 3 June 1999; In final form 28 April 2000)

Downloaded At: 10:08 22 January 2011

The fracture energy required to delaminate PMDA/ODA polyimide films from aluminum substrates was determined using the circular blister test. Films were prepared by spin coating the polyamic acid of PMDA and ODA onto polished aluminum substrates, by vapor co-deposition of PMDA and ODA monomers onto polished aluminum substrates, or by spin-coating the polyamic acid onto polished aluminum substrates that were first coated with thin layers of γ-aminopropyltriethoxysilane (γ-APS). Elastic and elastoplastic analyses were used to extract the fracture energies from the blister test results. Elastoplastic analysis provided fracture energies that ranged from 579 J/m^2 for spin-coated films on polished substrates to 705 J/m^2 for vapor-deposited films on polished substrates and to 750 J/m^2 for spin-coated films on silanated substrates. These values were intermediate between those provided by the two different elastic analyses. Differences in fracture energy determined by the three different analysis methods were related to plastic deformation in the films and, in the case of the two elastic analyses, to differences in the approach used to extract the fracture energy from experimental results. Failure of specimens prepared by spin-coating PMDA/ODA films onto aluminum substrates occurred cohesively within the polymer, near the interface between well imidized polymer in the bulk of the films and poorly imidized polymer in a layer near the aluminum surface. For the case of specimens prepared by vapor co-deposition of PMDA and ODA monomers, failure occurred within the vapor deposited films, close to the aluminum/film interface. Failure of spin-coated films on silanated substrates occurred mostly within the γ-APS but leaving "islands" of polyimide and silane on the aluminum.

---

*One of a Collection of papers honoring F. James Boerio, the recipient in February 1999 of *The Adhesion Society Award for Excellence in Adhesion Science, Sponsored by 3M.*

[†]Corresponding author. Tel.: 512-471-4164, Fax: 512-471-5500, e-mail: kml@mail.utexas.edu

Keywords: Polyimide/aluminum interphases; Cohesive zone model; Traction-separation law; Blister test; Interfacial fracture; Thin film delamination

INTRODUCTION

Polyimides are widely used in the microelectronics industry because of their good thermal, mechanical and chemical stability, excellent dielectric properties, and good film-forming characteristics [1 – 3]. Numerous investigations of the molecular structure of polyimide films as well as the interfacial structure and the adhesion of the films with various substrates have been reported. However, there have been few reports in which fracture mechanics methods have been applied to the delamination of polyimide films when the film/substrate "interphase" was carefully prepared and controlled. The purpose of this paper is to describe results that we have obtained using the circular blister test to determine the adhesive fracture toughness of polyimide/aluminum interphases. The interphases were prepared by spin-coating the polyamic acid of PMDA and ODA onto polished aluminum substrates, by vapor co-deposition of PMDA and ODA monomers onto polished aluminum substrates, and by spin-coating the polyamic acid onto polished aluminum substrates that were first coated with thin layers of γ-aminopropyltriethoxysilane (γ-APS). Elastic and elastoplastic analyses were used to extract the adhesive fracture energies from the experimental blister test results.

Most polyimides used in microelectronics are prepared by reaction of pyromellitic dianhydride (PMDA) and oxydianiline (ODA) to form a polyamic acid (PAA). Films are usually applied to substrates by spin-coating a solution of PAA in a strong solvent such as *n*-methyl-pyrollidone (NMP). The films are then heated to drive off the solvent and to convert the PAA to the corresponding polyimide. Alternatively, the PAA films can be chemically imidized. Chemical imidization is usually done by immersing polyamic acid films into acetic anhydride solutions that contain either pyridine or triethylamine. The base acts as a catalyst for the imidization reaction while acetic anhydride acts as a scavenger for water.

Many investigations of the molecular structure of interfaces between spin-coated polyimide films and metal substrates have been reported.

Downloaded At: 10:08 22 January 2011

Kim *et al.* [4, 5] used transmission electron microscopy (TEM) to investigate interfaces formed by thermal curing of polyamic acid spin-coated onto copper substrates. Cross-section TEM results showed small copper-rich particles distributed in the polyimide at distances greater than 80 - 200 nm from the copper surface. It was suggested that the polyamic acid reacted with copper to form a complex that decomposed during thermal imidization, resulting in the formation of copper-rich particles in the polyimide.

Burrell *et al.* [6] utilized XPS and IR to investigate thin films of polyimide prepared by spin-coating polyamic acids onto copper and aluminum substrates and then thermally imidizing the films. Films prepared on Al substrates were completely imidized during the heat treatment, as shown by XPS and IR measurements. Thus, the peaks near 284.6 and 286.0 eV in the C(1s) spectra of polyamic acid, which were assigned to carbon bound to other carbons or hydrogen and carbon bound to oxygen and nitrogen, respectively, appeared sharper in the C(1s) spectra of the polyimide film. Peaks near 287.9 and 289.0 eV due to carbonyl carbon in amide and acid groups merged into a single carbonyl component near 288.6 eV after thermal imidization. The O(1s) spectra showed a decrease in intensity of the C—O component relative to the C = O component. N(1s) spectra showed the appearance of a peak near 400.6 eV due to imide and the disappearance of a peak near 399.9 eV due to amide in polyamic acid. These observations indicated the formation of polyimide films on Al substrates. Reflection - absorption infrared (RAIR) spectra were characterized by bands near 1780 and 1730 cm^{-1} which were assigned to imide groups, supporting the conclusions obtained from the XPS investigation.

In the case of polyimide/copper interfaces, the C(1s) spectra exhibited several carbonyl components that were not related to the cured polyimide. The peak near 399.9 eV associated with the amide groups was still observed in N(1s) spectra. Peaks due to Cu(I) and Cu(II) were both present in the Cu(2p) spectra. In the infrared spectra of the polyimide on copper substrates, the band characteristic of imide functionality near 1730 cm^{-1} was not observed. Instead, a broad band near 1650 cm^{-1} was observed which was attributed to the superposition of the amide carbonyl band and one or more bands due to new chemical species. Another new band indicative of cuprous oxide

Downloaded At: 10:08 22 January 2011

was also observed near 640 cm^{-1}. As a result, it was proposed that copper/polyamic acid complexes were formed when polyamic acids were deposited onto copper substrates. A portion of these complexes was able to react with the amide group to yield imide groups plus oxide during thermal curing. However, formation of the copper/polyamic acid complex prevented films from curing completely during thermal treatment.

An alternative technique for forming polyimide films on metal substrates involves co-condensation of the monomers from the vapor onto the metal substrates. The monomers react rapidly on the surface to form polyamic acid, which may be thermally or chemically imidized. Films deposited in this manner fill small features better than spin coated films, but tend to follow the surface topology and do not planarize the surface as well as spin coated films [7, 8].

Several authors have investigated the vapor deposition of ultra-thin films of PMDA and ODA monomers onto various substrates [9–14]. PMDA appears to chemisorb onto silver and copper as a bidentate carboxylate salt [9, 13]. ODA monomer has been reported to fragment during adsorption onto silver [9]. It has also been reported that ODA physisorbs onto copper and silver surfaces [13, 14].

Grunze and Lamb [10, 15] used XPS to investigate vapor deposition of PMDA and ODA onto polycrystalline silver surfaces. PMDA and ODA were both chemisorbed on the silver surface through the oxygen atoms in the PMDA and ODA fragments. Co-deposition of PMDA and ODA followed by thermal treatment of the films led to formation of thermally-stable polyimide films. Peaks were observed near 286.2, 286.9, and 290.0 eV in the C(1s) spectra of co-deposited PMDA/ODA films having a thickness of about 11 Å. These peaks were assigned to aromatic carbon in the ODA, carbon in the PMDA ring and carbon attached to the nitrogen or oxygen in ODA, and carbonyl carbon, respectively. The calculated intensity ratio of these peaks was 4 : 9.5 : 9.6, while the ratio for a stoichiometric PMDA/ODA polyimide was 4 : 10 : 8. The relatively high intensity of the low binding energy C(1s) peak near 286.2 eV was explained by the presence of fragmented PMDA and ODA in the polyimide/silver interface. Contributions of fragmented PMDA and ODA to the spectra of the thin film were also evident in the O(1s) spectra where a peak near 531.5 eV was attributed to oxygen bonded directly to the silver surface. Therefore, it was

Downloaded At: 10:08 22 January 2011

concluded that the adhesion of polyimide films to silver surfaces involved bonding to fragments of PMDA and ODA, which were chemisorbed on the silver surface.

Other workers have described the vapor deposition of thick films onto silver surfaces [16]. Analysis with Raman spectroscopy suggested that the films were deposited as polyamic acid with a slight amount of ring closure to the imide structure. Heating at 200°C for 30 minutes resulted in films that were completely imidized and were spectroscopically identical to films of spin-coated PMDA/ODA.

Previous work also suggested that the *bulk* structure of vapor-deposited polyimides was very similar to that of spin-coated materials and that the qualitative adhesion to silicon was excellent [17]. However, the relationship between *interfacial* structure and the adhesion of vapor-deposited polyimide films to silicon and other substrates has not been reported.

Downloaded At: 10:08 22 January 2011

Adhesion promoters based on silane chemistry can be used to improve polymer/metal adhesion. Silane coupling agents have the general structure $X_3Si-R-Y$, where Y is an organofunctional group selected for bonding to specific organic polymers and X is a hydrolyzable group which forms silanol (SiOH) groups in aqueous solutions. Silanol groups are thought to be capable of reacting with mineral hydroxides (MOH) through hydrogen bonding or through condensation to form oxane (SiOM) bonds. The combination of strong, stable bonds between the polymer and the organofunctional groups and between the substrates and silanol groups improves the strength and durability of interfaces significantly.

Silane coupling agents are sometimes used to improve adhesion of polyimides to inorganic substrates [18]. In particular, γ-aminopropyltriethoxysilane (γ-APS) is used as an adhesion promoter for SiO_2/polymide interfaces. The mechanism by which aminosilanes enhance adhesion between SiO_2 and polyimides appears to involve formation of imide linkages between the polyamic acid and the primary amine of the adhesion promoter [19]. Although this must result in chain scission of the amic acid during ring closure, the strength and hydrothermal stability of these interfaces is significantly improved over that obtained from unsilanated surfaces.

The pressurized circular blister test configuration [20] was used to determine the adhesive fracture toughness of the different interphases

considered in this study. Gent and Lewandowski [21] used the results of a membrane analysis by Hencky [22] to analyze the elastic debonding of pressurized, thin circular blisters. As a result, the adhesive fracture energy can be determined from measurements of pressure and central deflection during debonding. Chu *et al.* [23, 24] extended the Gent and Lewandowski analysis so that, in constant flow rate experiments, only pressure-time histories following initiation needed to be measured in order to extract the adhesive fracture energy.

One concern with the test, especially for the film thicknesses that were used here, was that any determination of the adhesive fracture energy would be masked by the global plastic deformation in the blistering film. Unless accounted for, the accompanying plastic dissipation would mask the true values of the adhesive fracture energy as Kim and Aravas [25] showed in their analysis of steady state, elastoplastic peeling. Kinloch *et al.* [26] included the effect of crack tip rotation in a similar analysis and showed that it was an important effect for thin film peeling. More recently, Wei and Hutchinson [27] have made similar distinctions between the intrinsic toughness of an interface and plastic dissipation in transient thin film peeling by making use of a traction-separation law to represent the interface. This so-called fracture process zone model approach to analyzing interfacial crack growth problems was pioneered by Needleman [28, 29]. It has been used by Tvergaard and Hutchinson [30, 31] and Swadener and Liechti [32] to examine the role of plasticity in explaining the asymmetrical shielding effect [33] that occurs under shear-dominant loadings. The approach was also applied to circular blistering by Shirani and Liechti [34] in a companion paper that developed the procedures that will be used in this paper.

As indicated above, the purpose of this paper is to describe results that we have obtained using the circular blister test to determine the fracture energy required to delaminate PMDA/ODA films from aluminum substrates. Three different methods of film deposition were considered. In the first case, the polyamic acid of PMDA/ODA was spin-coated onto mechanically-polished and plasma-etched aluminum and then thermally imidized. In the second, the films were prepared similarly except that the substrates were first coated with thin films of γ-APS. The third type of film was prepared by vapor co-deposition of PMDA and ODA onto polished aluminum substrates. It will be shown

Downloaded At: 10:08 22 January 2011

that each deposition process produced a different interphase. In order to account for global plastic deformation of the films during blister testing, data obtained from several samples were analyzed using finite element analyses where the different interphases were essentially modeled as separate constitutive entities. This analysis allowed partitioning of the total energy release rate into components due to global plastic deformation and to other processes, including separation. The results gave insight into the nature of the mechanical properties of the interphase regions where failure occurred.

EXPERIMENTAL

This section is used to describe how the specimens were processed and how the fracture surfaces were analyzed. The blister experiment is also described.

Downloaded At: 10:08 22 January 2011

Specimen Preparation

Substrates for blister testing were prepared from 6061-T6 aluminum disks having a diameter of 101.6 mm and thickness of 25.4 mm. A hole having a diameter of 5.0 mm was drilled along the centerline of the substrate and threaded. This hole was used to pressurize the film/substrate interface during blister testing. It was threaded to facilitate connection to the pressurization system. The substrates were mechanically polished on 180, 400 and 600 grit SiC polishing discs and then on nylon cloths using 6.0 μm and 1.0 μm diamond polishing compound suspended in a hydrocarbon fluid. Between polishing steps, the substrates were thoroughly cleaned by wiping with acetone-soaked Kimwipes®.

After the final polishing and cleaning step, the hole along the centerline of the substrates was plugged with a thin disk of KBr formed *in-situ*. This provided a smooth surface for the subsequent application of films. Aluminum substrates were then placed in a capacitively-coupled radiofrequency (13.56 MHz) plasma reactor (Advanced Plasma Systems) and etched in an oxygen plasma at 500 mtorr pressure, 150 watts power, and 0.15 sccm total flow of oxygen.

After plasma cleaning, an aluminum substrate was affixed to the chuck of a spin-coater using double-sided adhesive tape. 2.5 ml of polyamic acid solution in *N,N*-dimethylpyrrolidone (NMP) (PI-2645D, DuPont Electronics) was flooded onto the surface of the substrate using a plastic syringe and the substrate was spun at 3000 rpm for 3–5 seconds. This resulted in the formation of a smooth, continuous film having a thickness of approximately 40 μm. The polyamic acid film was heated in an oven at 100°C in air for 1 hour to drive off the solvent and was then heated at 200°C for 1 hour in a N_2 atmosphere to convert the polyamic acid to polyimide. Although PMDA–ODA polyimides are usually cured at 350 to 400°C, curing the films at temperatures above 200°C destroyed the SERS substrates that were used for nondestructive evaluation of interphases. This means that comparing any data obtained in this study with others should be done with caution. The KBr plug was then dissolved in water and the substrate was connected to the pressurization system.

Some aluminum substrates were silanated before the polyamic acid was spin-coated. A 1.0% solution of γ-APS (Petrarch Systems, Inc.) in deionized water was prepared and allowed to hydrolyze for 5 minutes. A cleaned, polished aluminum substrate was immersed into the solution for 10 seconds, withdrawn, and blown dry using a stream of N_2. The substrate was then dried under vacuum in an oven at 100°C for 10 minutes to condense the γ-APS film on the aluminum surface. A film of the polyamic acid of PMDA/ODA was then spin-coated onto the silanated substrate and thermally imidized as described above.

In some cases, thin films of PMDA and ODA were deposited onto aluminum substrates by vapor co-deposition of the monomers using a modified diffusion-pumped thermal evaporator. Monomers were sublimed from independently heated aluminum crucibles. The evaporation crucibles were contained within a cylindrical aluminum baffle, equipped with a heater to prevent condensation of the vaporized monomer on its surface. The target substrate was suspended about 1 cm above the cylindrical baffle. Both the crucibles and the substrate base were equipped with chilled water cooling. This helped improve the rate of condensation on the substrate during deposition and allowed for rapid cool-down of the monomer crucibles at the end of a deposition cycle. Closed-loop PID temperature controllers controlled the temperatures of the crucibles, baffles, and substrate. System pressure during deposition was around 5×10^{-6} torr as measured with

Downloaded At: 10:08 22 January 2011

an ionization gauge located on the bell jar baseplate remote from the cylindrical baffle.

Vapor-deposited films were thermally imidized under nitrogen using the same temperature profile as for spin-coated films. However, the films were too thin for blister testing, so thick films of PMDA/ODA polyamic acid were spin-coated on top of them and thermally imidized, again using the same procedure. Prior to applying the overlayer, the vapor-deposited films were treated in an oxygen plasma to ensure adhesion of spin-coated polyimide. This procedure resulted in composite films with identical bulk mechanical properties to spin-coated films, but with a metal/polymer interface that consisted of vapor-deposited polyimide.

Fracture Surface Spectroscopy

Infrared microscopy was used to obtain reflection–absorption infrared (RAIR) spectra of the "substrate" failure surfaces of some blister test specimens and to determine the locus of failure. A Nic-Plan (Spectra-Tech) microscope equipped with a grazing angle objective lens and interfaced to a Magna 760 optical bench (Nicolet) was used to obtain the spectra. All spectra were obtained by averaging 512 scans at $8\,cm^{-1}$ spectral resolution. The spectrum of a clean, polished aluminum substrate was used as a baseline.

XPS spectra of the "substrate" and "polymer" failure surfaces were obtained using a Physical Electronics Model 5300 X-ray photoelectron spectrometer with Mg Kα radiation at a power of 300 W. The pass energy was 44.75 eV (0.5-eV step; 25-ms dwell time per step) and 17.90 (0.05-eV step; 50-ms dwell time per step) for the survey and high-resolution spectra, respectively. During analysis, the pressure was kept between 10^{-8} and 10^{-9} Torr. A take-off angle of 45° was used to obtain all spectra. The XPS spectra were corrected for charging by referencing the C(1s) peak of aliphatic and aromatic hydrocarbons to a value of 284.6 eV. Elemental compositions of the various surfaces were determined by integration of the areas under the individual elemental peaks in the high-resolution spectra. The spectra were fitted using a 90%/10% Gaussian/Lorentzian peak shape.

The thickness of the films was determined by using a Rudolph Research Model 436 ellipsometer to examine the metal substrates before and after deposition of the films. A computer program

Downloaded At: 10:08 22 January 2011

developed by McCrackin [35] was used to compute the film thickness from the ellipsometry parameters Δ and ψ.

Blister Apparatus

Figure 1 is a schematic view of the apparatus that was used for the blister experiment in this study. The pressurization system consisted of

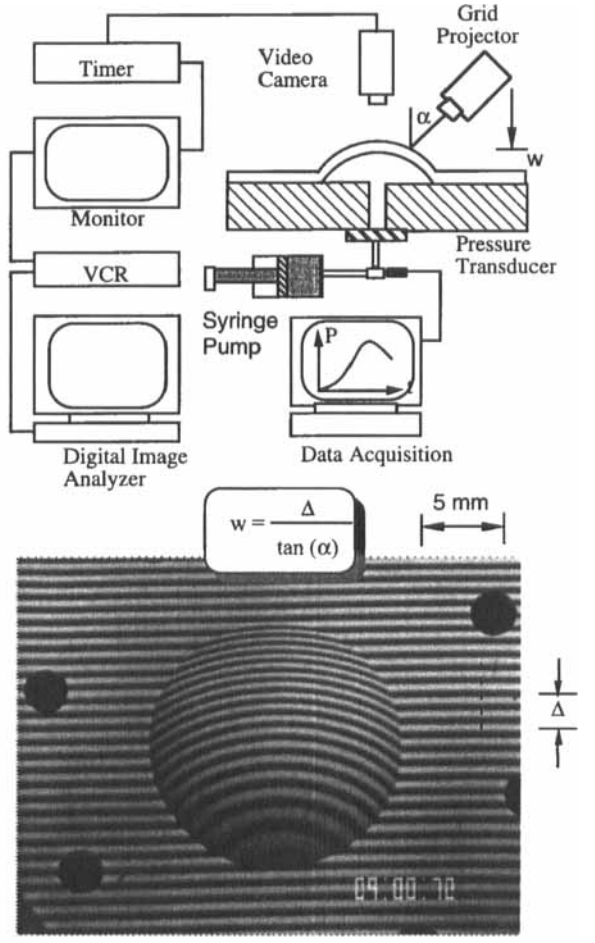

FIGURE 1 Circular blister apparatus.

Downloaded At: 10:08 22 January 2011

a syringe pump, a pressure transducer and deionized water. In order to minimize the effect of compliance, the components were designed to be as close as possible to one another. A syringe pump with flow rates ranging from 0.02 μl/hr to 500 ml/hr and with an accuracy of 0.5% with a 10 cc plastic syringe was used to control the volume flow rate of deionized water at 20 ml/hr. In most of the experiments, especially for blister initiation from the pressure porthole, an applied pressure up to 1.05 MPa was required, thereby ruling out the use of glass syringes. The resulting pressure was measured with a Sensotec pressure transducer with a resolution of 0.25% of full range and a maximum capacity of 1.38 MPa. The applied pressure was recorded by a computerized data acquisition system with 16-bit resolution. A video camera and recording system along with a digital image analyzer were used to measure the dimensions of the crack front and the change of volume of the blisters.

The projected grid method was adopted [34] for measuring the blister shape. The lateral deflection, Δ, of the lines (Fig. 1) is related to the out-of-plane displacement of the surface. The viewing from above provides a precise way of determining the shape of the crack front. Depending on the magnification that was being used, a light source with grids of 20, 10 or 5 lines/mm was used to project a shadow of the lines on the specimen. The video system recorded the change in line spacing while the test was in progress. Prior to each test, a two-dimensional calibration of length/pixel was necessary for each magnification level.

The following procedure was adopted for determining the deflection, w, of the blister at any particular location. The image analysis system was used to digitize recorded frames and then to scan the video image to obtain profiles of intensity of light *versus* pixel position. The location and order of the dark or bright lines were determined by identifying maxima and minima in the intensity profiles. The relative positions of the same bright or dark line in the undeformed and deformed configurations allowed the shift, Δ, to be determined. The deflection is related to the shift and the angle of illumination, α, through

$$w = \frac{\Delta}{\tan\alpha} \tag{1}$$

Downloaded At: 10:08 22 January 2011

The lines were projected at an angle of 30° giving rise to a resolution of 50 μm with a grating of 20 lines/mm by counting bright and dark lines, which could be located to within 0.1 mm. The overall accuracy of this technique was found to be 3% by using a calibrated 45° wedge [36].

Once the film displacement was determined, the change in volume, Δv, was obtained by integrating the area under the deflected shape in the following manner. First, the change in volume is given by

$$\Delta v = 2\pi \int_0^a w(r) r dr \tag{2}$$

where r is the distance from the center of the blister. In discrete form, Eq. (2) can be expressed as

$$\Delta v = 2\pi \sum_{i=1}^{n} \left(\frac{w_i - w_{i+1}}{2} \right) r_i \Delta r_i \tag{3}$$

where i denotes the ith data point.

In most experiments, crack growth was slow enough so that cracks, once initiated and grown for about 2 mm, could then be arrested by unloading, leaving a new starter crack for the next experiment. In this way, a single specimen could be used to conduct several experiments, so that enough data were obtained for each processing mode.

Downloaded At: 10:08 22 January 2011

ANALYSIS

In this section, we describe the steps that were taken to develop the analyses used to extract the adhesive fracture energies associated with the interphases that were created by the different processing routes. The first was an entirely elastic analysis of quasi-static debonding of a thin film from a rigid substrate following the approaches of Gent and Lewandowski [21] and Chu *et al.* [23, 24]. However, the kinematics were more general than those that were employed in the analysis of Hencky [22], which was the basis of the two analyses that were just referenced. The second was a finite element analysis that included the interface as a separate constitutive entity, while the polyimide was taken to be elastoplastic and the aluminum rigid. The details of the more general elastic analysis and the finite element analysis are given

in Shirani and Liechti [34]. The procedures and results are summarized here.

Elastic Debonding

The elastic debonding analysis was based on the stress analysis of a clamped plate that deformed radially and out-of-the plane with displacements u and w, respectively. As a result, the analysis essentially incorporated bending and membrane effects. In-plane residual stresses were also included in the analysis. However, for the range of blister radii and thicknesses and processing temperatures that were considered in the experiments conducted here, the membrane term is dominant, so that the volume change, Δv, is given by

$$\Delta v = C_1 \pi a^2 w_0 \tag{4}$$

where a and w_0 are the blister radius and central deflection, respectively. The constant in Eq. (4) depends on the boundary conditions and the Poisson's ratio of the film, which was 0.3. Under these conditions, the pressure (p) *vs.* central deflection (w_0) response is given by

$$w_0 = C_2 \left(\frac{pa^4}{Eh} \right)^{1/3} \tag{5}$$

where E is the Young's modulus and C_2 is also a coefficient whose values depend upon the value of Poisson's ratio, v, and the boundary conditions. For a Poisson's ratio of 0.3 and clamped boundaries, $C_1 = 0.519$ and $C_2 = 0.706$, which differ slightly from Hencky's [22] original result due to the inclusion of the radial displacement in the stress analysis. Equations (4) and (5) result in a pressure–volume response that is given by

$$p = \kappa (\Delta v)^3 \tag{6}$$

where $\kappa = [(C_1 C_2 \pi a)^3 (a/Eh)]^{-1}$.

Thus, for elastic deformations, the value of κ can be obtained from pressure and volume measurements, thereby allowing the Young's modulus to be extracted.

Downloaded At: 10:08 22 January 2011

Following the energy balance approach of Gent and Lewandowski [21] for a slowly propagating blister, albeit with slightly different kinematics, the adhesive fracture energy, Γ_a, can be related to the pressure and central deflection through,

$$\Gamma_a = C_3 p w_0, \tag{7}$$

where $C_3 = 0.619$ and is 4.6% lower than the value (0.649) from Gent and Lewandowski [21]. Thus, the adhesive fracture energy during elastic blistering can be determined from measurements of the pressure and central deflection.

Chu *et al.* [23, 24] expressed Eq. (7) in terms of pressure and time so that the central deflection would not have to be measured. This was achieved by introducing the volume flow rate so that a linear relationship between p^{-3} and time, t, results.

$$p^{-3} = \frac{R_f}{C_1 C_2 \pi}\left(\frac{Eh}{K_r^{10}}\right)^{1/3}(t - t_c) + p_c^{-3}, \tag{8}$$

where t_c is the time when debonding begins, p_c is the critical pressure, R_f is the constant volume rate of fluid injection and C_1 and C_2 are the coefficients from the membrane analysis in Eqs. (4) and (5). From Eq. (8), we can introduce the slope, N_s, of the plot of p^{-3} *vs.* $(t - t_c)$ as

$$N_s = \frac{R_f}{C_1 C_2 \pi}\left(\frac{Eh}{K_r^{10}}\right)^{1/3}. \tag{9}$$

The constant K_r was obtained from Eq. (16) of [21], which applies to the quasi-static debonding stage of the experiments. For this analysis

$$K_r = (C_4 E h \Gamma_a^3)^{1/4}, \tag{10}$$

where

$$C_4 = \left(\frac{4}{5 C_1 C_2}\right)^3. \tag{11}$$

Downloaded At: 10:08 22 January 2011

The value of N_s can be extracted from each experiment. Combining Eqs. (9) and (10), one finds that

$$\Gamma_a = C_5 \left[\frac{R_f^2}{N_s^2 E h} \right]^{1/5}, \tag{12}$$

where

$$C_5 = \frac{1}{\sqrt[3]{C_4}} \left[\frac{1}{(C_1 C_2 \pi)^2} \right]^{1/5}. \tag{13}$$

The analysis of Shirani and Liechti [34] yielded $C_5 = 0.431$ compared with $C_5 = 0.395$ based on the kinematics used in Ref. [21]. This leads to a 9% difference in Γ_a values.

Nonetheless, it can be seen from Eq. (12) that the adhesive fracture energy, Γ_a, can be determined from measurements of the pressure history (N_s) and the rate of fluid injection (R_f). This greatly simplifies the data reduction process, because a height or volume measurement is not required, if the loading device compliance is low.

Paek and Durning [37] have recently conducted an analysis of circular blistering when the delaminating film is neo-Hookean and the kinematics are those of a spherical cap. The analysis indicated that delamination under volume control is still stable.

Elastoplastic Debonding

In Liechti and Shirani [38], it was shown that large scale yielding (spanning the film thickness, but not necessarily the whole blister diameter) could occur in circular blister specimens with an adhesive fracture energy of 100 J/m^2. In some cases, there was complete yielding of the delaminating film, so that J-dominance would no longer apply. In order to account for the large amount of yielding and still extract the adhesive fracture energy, the fracture process zone approach of Needleman [28, 29] and Tvergaard and Hutchinson [30, 31] was adopted by Shirani and Liechti [34] for the analysis of circular blisters. This approach essentially involves attributing a traction-separation law to the interface and, because it allows crack growth to occur, the associated plastic dissipation from loading and unloading of

Downloaded At: 10:08 22 January 2011

points that are passed by the crack front is accounted for. As a result, the area determines the adhesive fracture energy under the chosen traction-separation law. The dominant scale of the fracture process zone in many interface systems can, indeed, be measured in microns rather than nanometers. Thus, the traction-separation law for an interface should be regarded as a phenomenological characterization of the zone where the separation takes place along the interface and not necessarily a description of atomic separation. As the experimental results will show later, the traction separation laws obtained here represent the deformation characteristics of the different interphase regions that were formed.

The projected grid measurements indicated clearly that the crack front was circular. An axisymmetric analysis was, therefore, conducted (using the finite element code ABAQUS) by considering the aluminum to be rigid and using four-node shell elements to represent the polyimide layer. The polyimide was modeled as a J_2 flow theory material with isotropic hardening. A Ramberg Osgood fit with parameters n and σ_0 derived from bulge tests [34] was used to represent the stress–strain curve.

Spring elements in the ABAQUS finite element code were used to simulate the traction separation laws in the directions normal and tangential to the interface. The particular values of the parameters of the traction-separation law were chosen by making fits to pressure-volume and crack opening displacement data.

The separation law of the interface contains a number of parameters: the adhesive fracture energy, Γ_a, the value of peak stress, $\tilde{\sigma}$, the critical displacement ratio (δ_n^c/δ_t^c) (subscripts n and t, respectively, refer to the normal and tangential directions to the interface), along with others that define its shape. Earlier studies by Tvergaard and Hutchinson [30] and several cases that were considered [34] suggest that the details of the shape of the separation law are relatively unimportant. As a result, we considered an essentially triangular traction separation law so that

$$\Gamma_a \cong \frac{1}{2}\tilde{\sigma}\delta_n^c \tag{13}$$

which shows that Γ_a and $\tilde{\sigma}$ are the two most important parameters for characterizing the fracture process in this model. The study on

Downloaded At: 10:08 22 January 2011

mixed-mode interface toughness using this model [31] showed that the predictions do not seem to be very sensitive to other features of the traction-separation law, such as the relative peak in the shear traction to normal traction as specified by the parameter (δ_n^c/δ_t^c), which we, therefore, took to be unity. Use of the potential function ensures that the work of separation, Γ_a, is independent of the combination of normal and tangential displacements taking place in the process zone.

The values of Γ_a and $\tilde{\sigma}$ for each interphase were determined in an iterative manner by comparing the predicted pressure–volume responses and the crack opening displacements (COD) with the measured ones. About 10 iterations were usually required in order to obtain a reasonable fit to the data. The sensitivity of the responses to the choices of Γ_a and $\tilde{\sigma}$ was examined by Shirani and Liechti [34].

Downloaded At: 10:08 22 January 2011

RESULTS AND DISCUSSION

Four specimens (designated *A*, *B*, *C* and *D*) were used in the study. Specimen *A* was prepared by spin-coating polyamic acid on the aluminum and imidizing. Specimens *B* and *C* were prepared *via* vapor deposition and then spin-coating. It was later discovered that specimen *B* had been contaminated. Nevertheless, it provided us with another surface for which to determine the traction-separation law. Unfortunately, no attempt could be made to link the contamination to the traction-separation law. Specimen *D* had the silane treatment followed by spin-coating. The thicknesses of the films are tabulated below.

The pressure histories of the four specimen types are compared in Figure 2. In each case, the highest pressures were experienced during the first experiment where the crack was not sharp. The initial experiment was useful for determining the stress strain behavior of the polyimide for each method of applying the polyimide. The properties obtained from the bulge tests are given in Table II. No significant differences were encountered from specimen to specimen.

The subsequent experiments on each specimen type produced stable, quasi-static growth in all cases. Only three such runs could be made with the silane-treated specimen (*D*) due to a pinhole in the specimen that caused a leak.

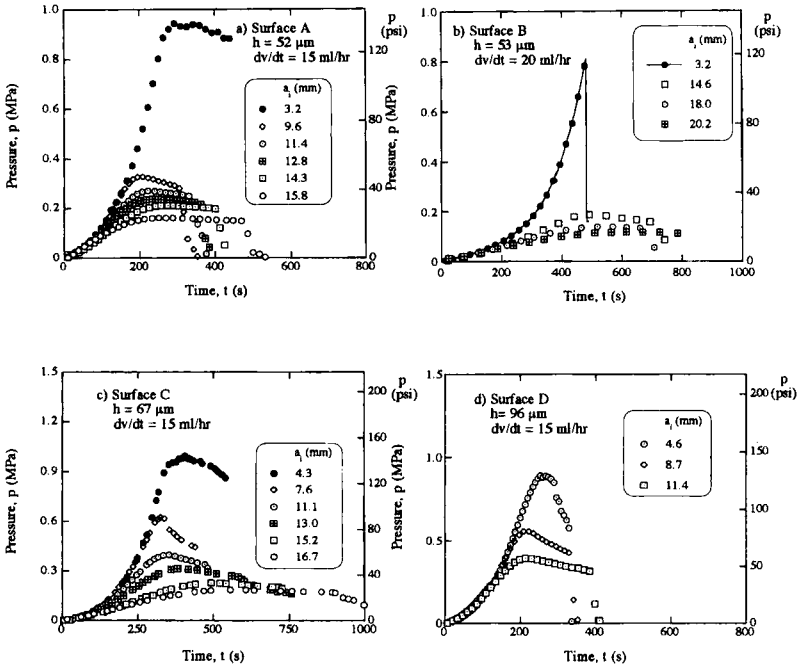

FIGURE 2 Pressure histories of the four specimens.

TABLE I Blister thicknesses

Specimen	*Specimen preparation*	*Thickness* (μm)
A	Spin-coat PMDA/ODA	52
B	Vapor deposition plus spin-coat (contaminated)	53
C	Vapor deposition plus spin-coat	67
D	Silane plus spin-coat	96

TABLE II The mechanical properties of polyimide PMDA/ODA

Young's modulus, E (GPa)	*Yield stress,* σ_y *(MPa)*	*Ramberg Osgood exponent, n*	*Ramberg Osgood stress,* σ_0 *(MPa)*
2.15	31	5.85	26

The shape and deformation of each blister were measured as described earlier. Blisters *A* and *B* were circular from beginning to end, growing in an entirely self-similar manner. Blister *C* maintained a

Downloaded At: 10:08 22 January 2011

nearly circular crack front but grew in a preferential direction due to a concomitant thinning of the film. The initial crack front in D was irregular but subsequent crack fronts were very circular. The measured central displacements were used to construct the pressure *vs.* displacement responses shown in Figure 3. The corresponding predictions for a single growing crack are also shown. The jagged nature of the predictions was due to the way the traction separation law was discretized [34]. In each case, the traction-separation law of the interface was adjusted to match the debonding response that had been measured in the experiments. The measured inflation response prior to the initial blow-off matched [34] the expected Gent and Lewandowski [21] cubic relationship. However, the measured inflation responses prior to stable growth in the subsequent experiments tended to be initially much stiffer than that of the expected cubic relation. Residual stresses do stiffen the pressure-displacement responses of pressurized films [36] but not to the extent that was experienced in the experiments. Although the unloading responses were not fully measured in all cases,

Downloaded At: 10:08 22 January 2011

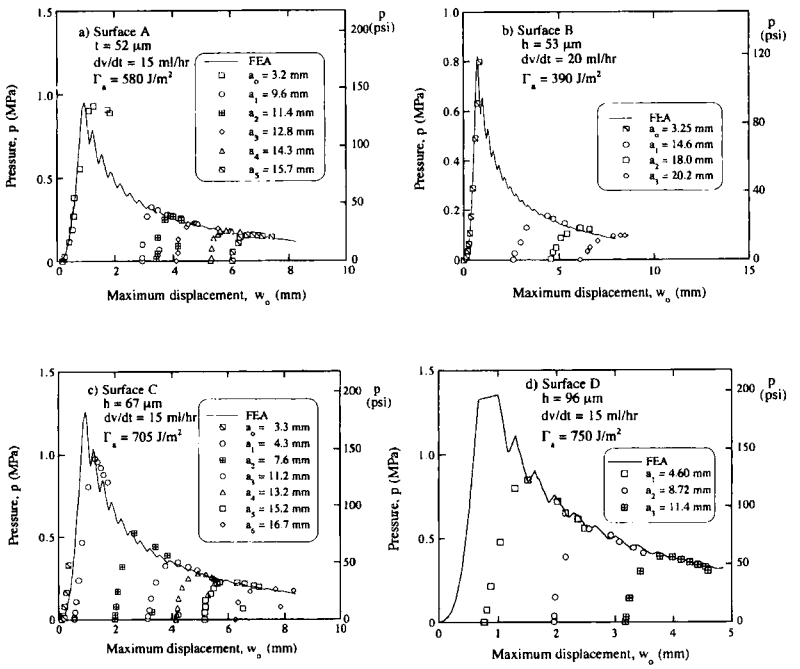

FIGURE 3 Pressure *vs.* central displacement responses of the four specimens.

there were signs of hysteresis (Fig. 3c). Both observations are consistent with viscoelastic effects, which could not be accounted for at this time. However, these effects were probably small during steady state propagation, which was used to establish the process zone parameters.

Adhesive Fracture Energies

The adhesive fracture energies that were obtained from the elastic and elsastoplastic analyses are now presented and compared. The results from the elastic analyses come from Eqs. (7) and (12). The elastoplastic results are from the finite element analyses.

Elastic Analyses

The values of adhesive fracture energy obtained from Eq. (7), which is valid for $\Delta a > 0$, are plotted against crack radius in Figure 4. The values of energy release rate prior to crack extension ($\Delta a = 0$) were obtained from Eq. (2.21) in [36]. Together, the two equations essentially produce the resistance curves that can be seen in Figure 4.

For surface treatments *A* and *B*, the adhesive fracture energies quickly reached steady state. The steady state values of treatment *A* were consistent from experiment to experiment, whereas those associated with treatment *B* rose slightly with increasing initial crack radius. The stable crack growth portions of the resistance curves for preparations *C* and *D* were longer due to the higher toughnesses. If anything, there was a slight drop in the steady state values for surface *C* in going from experiment to experiment. This may have been due to the slight (unaccounted for) changes in thickness referred to earlier. The resistance curves for preparation *D* had distinctive maxima but were consistent throughout the experiments.

The average of the adhesive fracture energy values was taken from the steady state values across all experiments with each surface treatment. Table III compares the values extracted in this way with the averages that were obtained by applying Eq. (12), which will be discussed shortly. From the second column, we see that specimen *B* had the most brittle interphase. This was apparently due to some contamination that was introduced during its processing. The toughest

Downloaded At: 10:08 22 January 2011

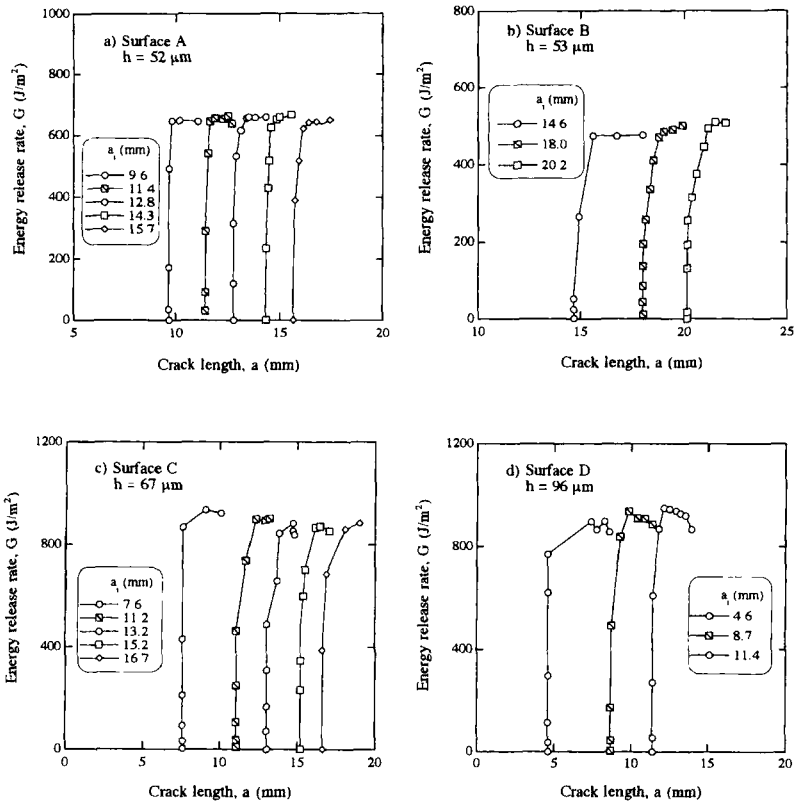

FIGURE 4 Resistance curves based on Eq. (7) during growth.

TABLE III Comparison of average adhesive fracture energies from elastic analyses

Surface	Γ_a (J/m^2) *Eq.* (7)	Γ_a (J/m^2) *Eq.* (12)	*Error** %
A	646	530	22
B	510	313	63
C	883	671	32
D	901	700	29

* $\Gamma_a(7) - \Gamma_a(12)$ · $\Gamma_a(12)$.

interphase was the one that was produced by the silane treatment (*D*), although vapor deposition (*C*) resulted in an adhesive fracture energy value that was not much lower.

Downloaded At: 10:08 22 January 2011

Shown in the third column are the toughness values that were obtained from Eq. (12) and from the pressure-time histories (Fig. 3) that were obtained in the initial pressurization and subsequent delamination experiments. In all cases except preparation *D*, the pressure levels encountered during subsequent experiments were considerably lower. The initial blister in preparation *D* was irregular but became circular for the subsequent experiments. The corresponding p^{-3} *vs.* *t* plots are shown in Figure 5 and the extracted values of Γ_a are compared in Table III. The data shown in Figures 5a, b and c were for the linear portion. When all the data were plotted [34], the response immediately following initiation was usually nonlinear. These plots yielded consistent values of adhesive fracture energy for each surface treatment.

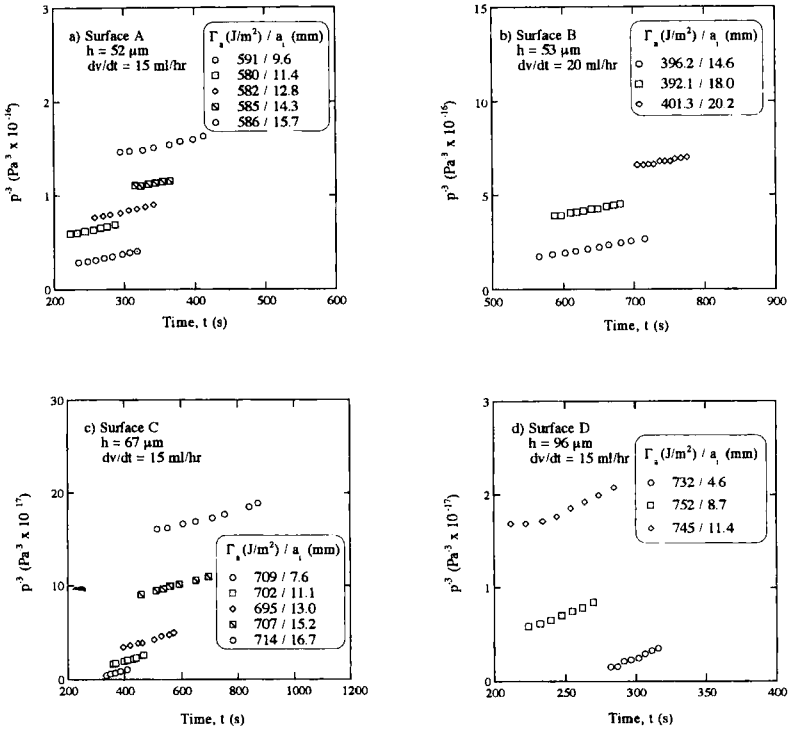

FIGURE 5 Linear fit of $p^{-1/3}$ *vs.* time for the four specimens.

Downloaded At: 10:08 22 January 2011

The values of adhesive fracture energy that are listed in column 2 of Table III were calculated based on the volume flow rates of fluid which were extracted experimentally and are shown in Table IV. These volume rates are lower than the nominal applied volume rates for each specimen and, consequently, yield lower adhesive fracture energies from Eq. (12).

It can be seen (Tab. III) that the contaminated surface *B* gave rise to the lowest adhesive fracture energy. The adhesive fracture toughness of the basic surface (preparation *A*) was lower than the values obtained by vapor deposition of polyimide and silane treatment. The latter provided the highest adhesive fracture energy at 700.1 J/m^2.

While the ranking of surface treatments was still the same, the adhesive fracture energies from Eq. (12) were consistently lower than those from Eq. (7). The percentage difference with respect to the values obtained from Eq. (12) ranged from 21.8 to 63.2%. These values of the adhesive fracture energies will now be compared with the results from the cohesive zone modeling.

Downloaded At: 10:08 22 January 2011

Elastoplastic Analysis

The predicted pressure *vs.* central deflection responses from the elastoplastic analyses are compared with the measured values in Figure 3. In all cases, the match in responses during the propagation phase was good, indicating that a reasonable choice of interfacial constitutive behavior had been made for each surface treatment. This was further confirmed in comparisons of crack opening displacement data and predictions (Fig. 6). The predictions matched both the crack radius and the crack opening displacements.

The total fracture energy, adhesive fracture energy and plastic dissipation rate for each surface are plotted in Figure 7. The adhesive

TABLE IV Volume rates for each surface treatment

Specimen	*A*	*B*	*C*	*D*
Actual volume rate (mm^3/s)	3.433	4.074	3.879	3.726
Nominal volume rate (mm^3/s)	4.167	5.556	4.167	4.167
Error (%)	17.6	26.7	6.9	10.6

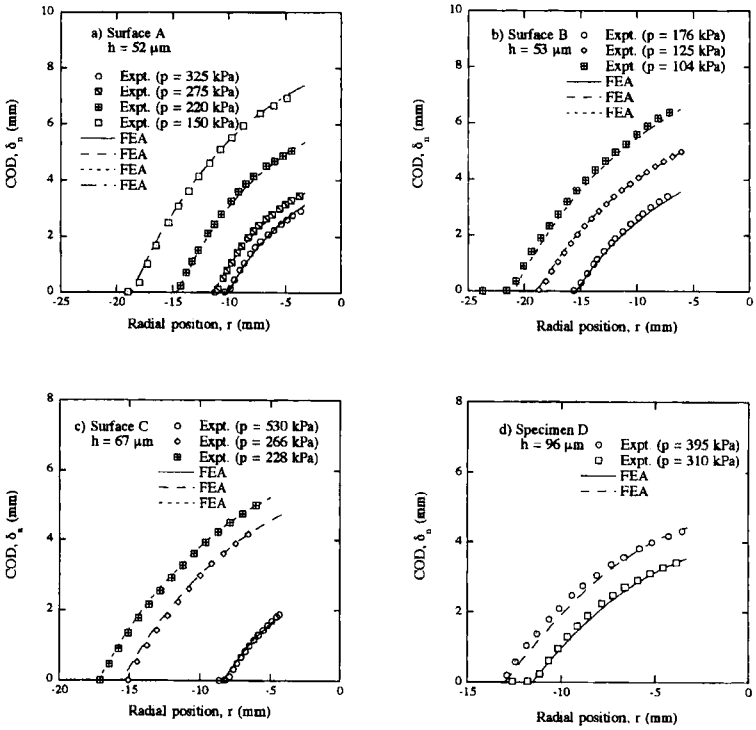

FIGURE 6 Comparison of measured and predicted crack opening displacements.

fracture energies are compared (Tab. V) with those that were extracted *via* Eqs. (7) and (12).

The values of adhesive fracture energies that were obtained from Eq. (12) were 7 to 20% lower than the values obtained from the springs that were chosen for the cohesive zone model. On the other hand, the adhesive fracture energies extracted from Eq. (7) were all higher than the values extracted from Eq. (12) and the finite element analysis. The reason for the higher Γ_a values from Eq. (7) is that, although the analysis was elastic, it was applied to the measured pressures and central displacements. Since yielding was experienced in the experiments, the central displacements are higher than their elastic counterparts at a given pressure, thereby leading to higher Γ_a values. This is confirmed by the fact that the values of adhesive fracture energy derived from Eq. (7) were close to the Γ_t values obtained from the finite element analyses, and plastic dissipation is included in Γ_t.

Downloaded At: 10:08 22 January 2011

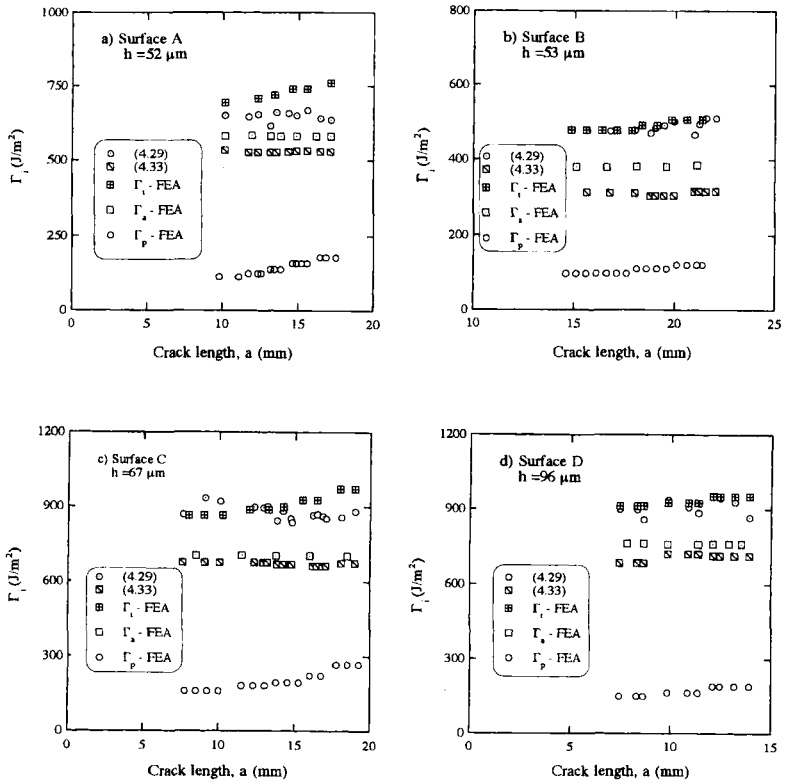

FIGURE 7 Comparison of total energy release rates, adhesive fracture energies and plastic dissipation in the four specimens.

TABLE V Comparison of adhesive fracture energies

Surface	Γ_a (J/m^2) *Eq.* (7)	Γ_a (J/m^2) *Eq.* (12)	Γ_a (J/m^2) *CZM*	$\tilde{\sigma}/\sigma_y$ *CZM*
A	646	530	579	6.3
B	511	313	390	4.6
C	883	671	705	7.5
D	901	700	750	8.1

At the same time, it is initially surprising that the values of adhesive fracture energies obtained from Eq. (12) and Figure 5 were so much lower than the values from Eq. (7). Equation (12) was derived from the elastic analysis that led to Eq. (7) and essentially uses the volume flow rate instead of the central displacement. However, the volume flow rate is (in spite of some machine compliance) the independent variable,

Downloaded At: 10:08 22 January 2011

which means that it is not affected by any inelastic response of the film. As a result, the values of adhesive fracture energy that were obtained from Eq. (12) and the data in Figure 5 were quite close to the values that were derived from the finite element analysis.

On the basis of the cohesive zone model, we see (Tab. V) that the silane treatment (*D*) resulted in the largest adhesive fracture energy (750 J/m^2). The vapor-deposited polyimide interface was a close second at 705 J/m^2. The spin-coated polyimide (*A*) gave rise to an adhesive fracture energy of 590 J/m^2, while the contaminated surface (*B*) had the lowest adhesive fracture energy at 390 J/m^2. These values are all lower than the fracture toughness of neat polyimide in bulk form, which is about 1 kJ/m^2. They are also much greater than the thermodynamic work of adhesion, which is of the order of 0.1 J/m^2. We can conclude that the cohesive zone model is apparently representing the toughness of the material in the fracture plane. As a result, indications are that the material near the fracture plane differed from the bulk, as will be seen from spectroscopic analyses of the fracture surfaces that will be discussed later.

Also shown in Table V are the maximum traction levels (normalized by the yield strength of the polyimide) that were used in the traction-separation laws for each interface. The ranking of the different surfaces based on maximum traction levels correspond to those based on adhesive fracture energy. The values are quite large compared with those that were used in the examples of Tvergaard and Hutchinson [31]. Such high strengths may be possible on the small scale of the interphases. They may also be an artifact of the cohesive zone modeling process, as pointed out by Tvergaard and Hutchinson.

The distinction between surfaces *C* and *D* was lost when the total fracture energy was considered (Fig. 8). This was because the thickness of the polyimide layer in specimen *C* was smaller and the increase in the amount of plastic dissipation was sufficient to overcome the differential in adhesive fracture energies that was noted in Table V. The plastic dissipation rates are compared in Figure 9. The increase in plastic dissipation rate with crack radius is very striking in all cases. The film thickness effect can also be seen by comparing the responses of specimens *C* and *D*. The specimen with the thinner film (*C*) and the lower adhesive fracture energy had slightly more plastic dissipation. Specimens *A* and *B* had almost the same film thickness (52 and 53 μm,

Downloaded At: 10:08 22 January 2011

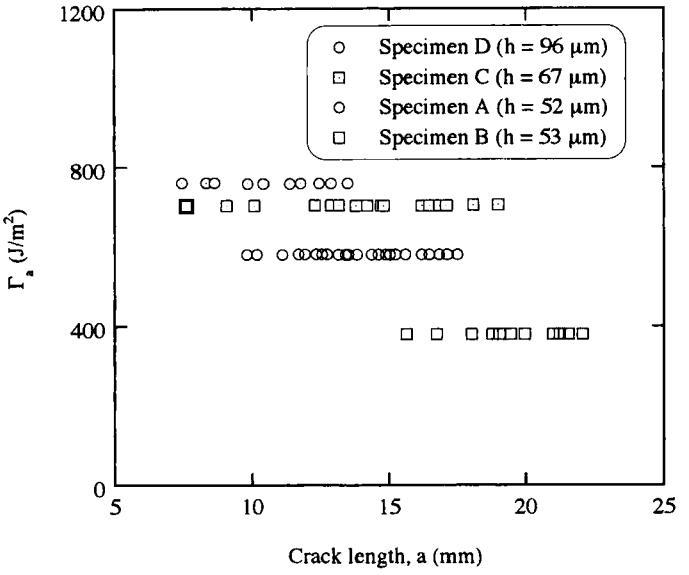

FIGURE 8 Adhesive fracture energies of the four specimens.

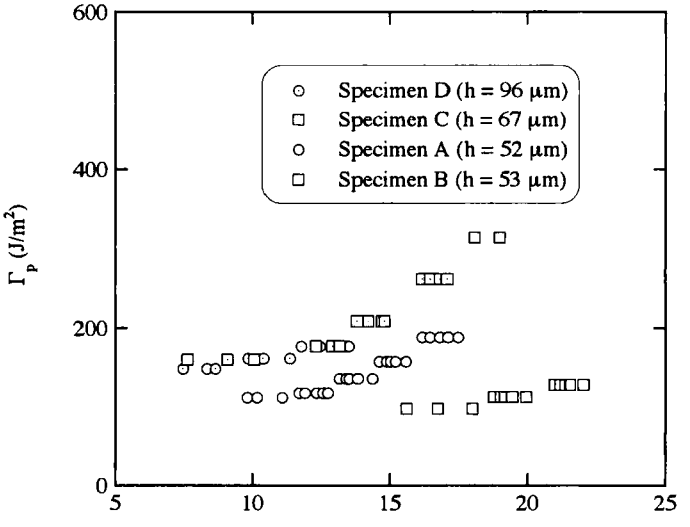

FIGURE 9 Plastic dissipation in the four specimens.

Downloaded At: 10:08 22 January 2011

respectively) but, since surface *A* had a higher adhesive fracture energy and required higher pressures for delamination, the global plastic dissipation rates were higher. When the global plastic dissipation was normalized by the adhesive fracture energy (Fig. 10), the percentages ranged from 19 to 38%. The largest amount of relative plastic dissipation occurred in specimen *C*, due to its relatively high adhesive fracture energy and lower film thickness. Even though specimen *D* had the highest adhesive fracture energy, it had the thickest film of all the specimens and the relative amount of yielding was on a par with that of specimens *A* and *B*.

Spectroscopic Analysis of Failure Surfaces

Sample A (PMDA/ODA Spin-coated onto Aluminum)

The XPS survey spectra of the polymer and aluminum failure surfaces of a blister test specimen that was prepared by spin-coating the polyamic acid of PMDA/ODA onto aluminum and then thermally

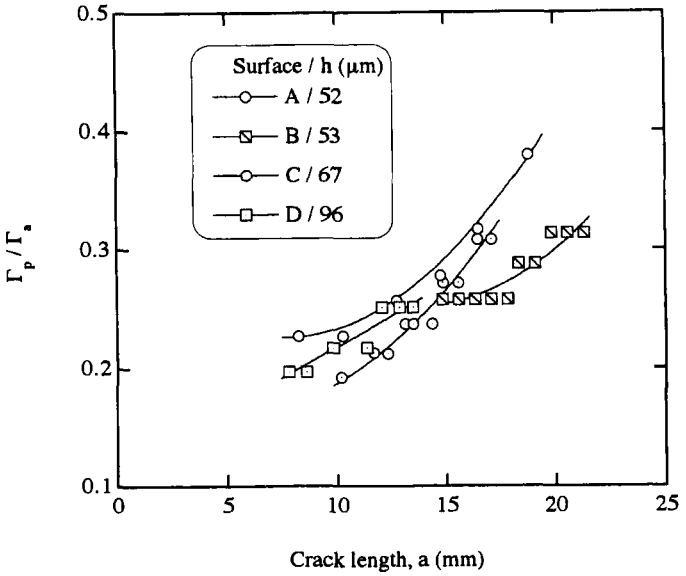

FIGURE 10 Relative amount of global plastic dissipation in each of the four specimens.

Downloaded At: 10:08 22 January 2011

imidizing the polyamic acid are shown in Figure 11. The elemental composition for the polymer failure surface was 74.3% carbon, 19.2% oxygen, and 6.5% nitrogen, while that of the aluminum failure surface was 46.7% carbon, 37.6% oxygen, 3.4% nitrogen, and 12.2% aluminum. Observation of peaks due to aluminum and nitrogen in the spectrum of the aluminum failure surface indicated that failure was close to the substrate surface and that some polymer remained on the substrate.

High-resolution C(1s) and N(1s) XPS spectra for the polymer failure surface are shown in Figures 12 and 13, respectively. The C(1s) spectrum was typical of a highly-imidized polyimide and consisted of five components [39]. The main peak at 284.6 eV was assigned to aromatic carbon atoms. The strong peak shifted upward from the main peak by 1.0 eV was assigned to carbon atoms singly bonded to nitrogen (C—N) and to the carbon atoms in the aromatic rings of the PMDA moieties. The C(1s) binding energy of these aromatic carbon atoms was shifted upward from its usual position near 284.6 eV by the electron withdrawing effect of the imide rings. The peak shifted upward by 1.7 eV was assigned to aromatic carbon atoms singly bonded to oxygen (C—O). Components shifted upward by 4.0 eV and

Downloaded At: 10:08 22 January 2011

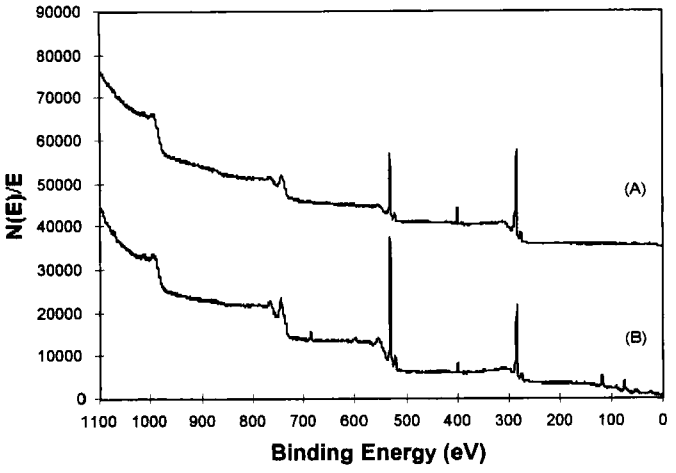

FIGURE 11 XPS survey spectra of (A) – polymer and (B) – aluminum failure surfaces of a blister test specimen that was prepared by spin-coating the polyamic acid of PMDA/ODA onto aluminum and then thermally imidizing the polyamic acid.

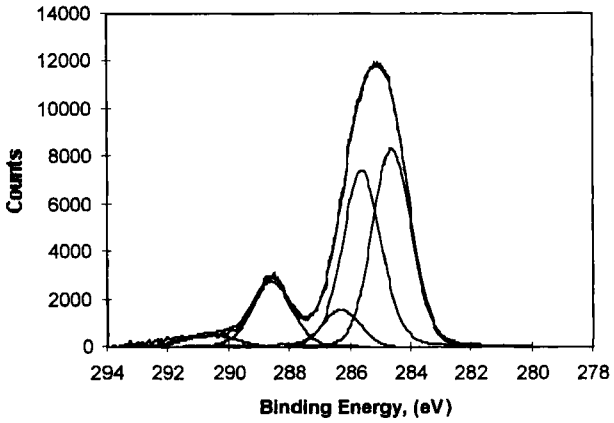

Peak position, eV	Separation, eV	% of total area	FWHM	Assignment
284.6	0.0	39.6	1.45	C-C, C-H
285.6	1.0	34.5	1.45	C-N + C-imide
286.3	1.7	10.4	1.45	C-O-C
288.6	4.0	12.7	1.45	imide C=O
290.7	6.1	2.8	2.00	$\pi \rightarrow \pi^*$

FIGURE 12 High-resolution C(1s) XPS spectra for the polymer failure surface of a blister test specimen that was prepared by spin-coating the polyamic acid of PMDA/ODA onto aluminum and then thermally imidizing the polyamic acid.

Downloaded At: 10:08 22 January 2011

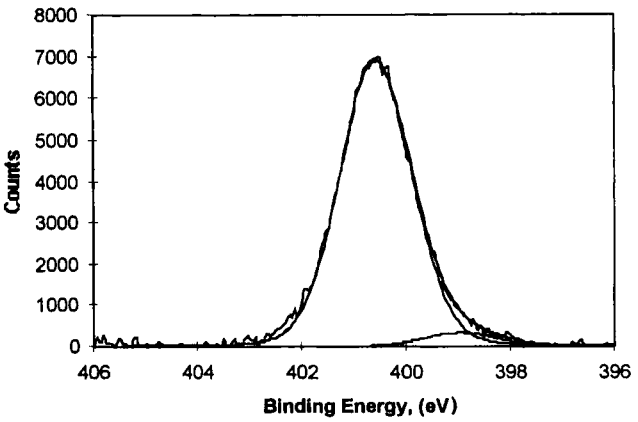

Peak position, eV	Separation, eV	% of total area	Assignment
400.6	0.00	95.4	Imide
399.0	-1.6	4.6	Isoimide

FIGURE 13 XPS high-resolution spectrum of the N(1s) region of the polymer failure surface of a blister test specimen that was prepared by spin-coating the polyamic acid of PMDA/ODA onto aluminum and then thermally imidizing the polyamic acid.

6.1 eV were characteristic of carbonyl groups in imide rings and the $\pi \rightarrow \pi^*$ transition of carbon atoms in the aromatic rings, respectively.

By comparison, the C(1s) spectrum of the neat polyamic acid consists of six components. A strong band due to carbon atoms in the aromatic rings is located at 284.6 eV. There are additional weak bands shifted upward in binding energy by 0.9, 1.7, 3.1, 4.5 and 5.9 eV that are assigned to C—N, C—O, carbon atoms in amide groups, carbon atoms in acid groups, and $\pi \rightarrow \pi^*$ transitions of aromatic carbon atoms, respectively.

The spectrum in Figure 13 shows that the N(1s) binding energy was about 400.5 eV. Considering that the N(1s) binding energy is about 399.5 eV for the polyamic acid and 400.3 eV for the polyimide, it was evident that the polymer failure surface consisted of well-imidized polyimide. This conclusion was consistent with that reached from an analysis of the C(1s) spectra.

The C(1s) and N(1s) XPS spectra for the aluminum failure surface are shown in Figures 14 and 15, respectively. The C(1s) spectrum was

Downloaded At: 10:08 22 January 2011

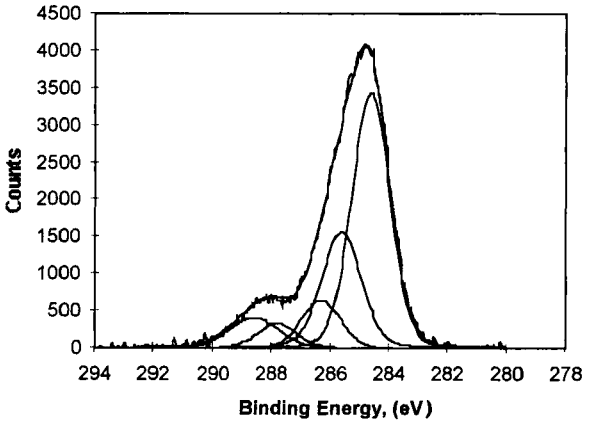

Peak position, eV	Separation, eV	% of total area	FWHM	Assignment
284.6	0.0	52.2	1.50	C-C, C-H
285.6	1.0	22.4	1.50	C-N + C-imide
286.3	1.7	11.8	1.50	C-O-C
287.7	3.1	5.9	1.50	amide, COO^-
288.6	4.0	7.9	1.50	imide C=O

FIGURE 14 XPS high-resolution spectrum of the C(1s) region of the aluminum failure surface of a blister test specimen that was prepared by spin-coating the polyamic acid of PMDA/ODA onto aluminum and then thermally imidizing the polyamic acid.

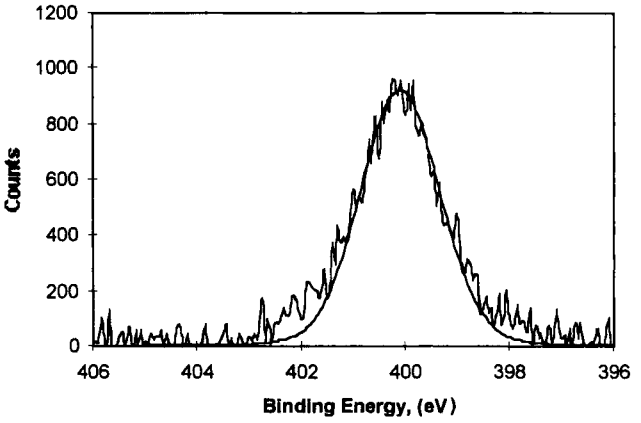

Peak position, eV	Separation, eV	% of total area	Assignment
400.1	0.0	100	amide

FIGURE 15 XPS high-resolution N(1s) spectrum of the aluminum failure surface of a blister test specimen that was prepared by spin-coating the polyamic acid of MPDA/ODA onto aluminum and then thermally imidizing the polyamic acid.

Downloaded At: 10:08 22 January 2011

composed of five components characteristic of polyamic acid or poorly-imidized polyimide. The main aromatic carbon peak was present at 284.6 eV. The peak shifted upward by 1.0 eV was assigned to C—N and to aromatic carbon atoms with their C(1s) binding energy shifted upward by the electron-withdrawing effect of imide rings. However, this component was less intense in the C(1s) spectrum of the aluminum failure surface than in the spectrum of the polymer failure surface (Fig. 12), indicating less formation of imide rings in the polymer remaining on the aluminum failure surface. Further evidence for limited imide formation on the aluminum failure surface was provided by the observation of a component in the C(1s) spectrum that was shifted upward from the main peak by about 3.1 eV and assigned to carboxylate species. Some evidence for imide formation was provided by the observation of components in the C(1s) spectrum that were shifted upward from the main peak by 1.7 and 4.0 eV and assigned to C—O and imide carbonyl, respectively. The N(1s) spectrum of the polymer remaining on the aluminum failure surface (Fig. 15) consisted of a strong band near 400.2 eV and a very weak

band near 399.0 eV which were assigned to carbon atoms in imide carbonyl groups and isoimide groups, respectively. The relatively low binding energy of the main N(1s) band confirmed that polymer remaining on the aluminum failure surface was only partly imidized.

From these results, it was evident that the fracture plane of blister test specimens prepared by spin-coating PMDA/ODA films onto aluminum substrates was cohesive within the polymer, near the interface between well-imidized polymer in the bulk of the film and poorly-imidized polymer in a layer near the aluminum surface. The interaction of the aluminum ions on the substrate surface and the polyamic acid adjacent to the substrate formed carboxylate salts, which hindered imidization of the polyamic acid.

Sample C – PMDA/ODA Vapor Deposited and Spin-coated onto Aluminum

The elemental composition of the polymer failure surface was 74.8% carbon, 18.9% oxygen, 5.6% nitrogen, and 0.7% aluminum. For the aluminum failure surface, the elemental composition was 50.0% carbon, 32.8% oxygen, 4.7% nitrogen, and 12.6% aluminum. Aluminum was present on both the polymer and aluminum failure surfaces, indicating that failure occurred very close to the interface between the vapor-deposited film and the aluminum substrate.

High-resolution C(1s) and N(1s) XPS spectra of the polymer failure surface were similar to the spectra shown in Figures 12 and 13, respectively. The C(1s) spectra consisted of the five peaks characteristic of well-imidized polyimide. They included a strong band at 284.6 eV, assigned to aromatic carbon atoms, and a strong peak shifted upward in binding energy by 1.0 eV that was assigned to C—N and to the electron-withdrawing effect of the imide rings on the carbon atoms in the PMDA moieties. A peak shifted by 1.7 eV was assigned to the aromatic carbon singly bonded to oxygen. Peaks shifted upward from the main hydrocarbon peak by 4.0 eV and 6.1 eV were characteristic of the imide carbonyl group and the $\pi \rightarrow \pi^*$ double bond transition from the aromatic rings, respectively.

The N(1s) spectrum consisted of a strong band near 400.6 eV and a weak band near 399.0 eV. The band near 400.6 eV was again indicative

Downloaded At: 10:08 22 January 2011

of well-imidized material on the polymer failure surface while the band near 399.0 eV indicated the formation of a small amount of isoimide.

C(1s) and N(1s) high-resolution XPS spectra for the aluminum failure surface were also similar to the spectra shown in Figures 12 and 13, respectively. Both spectra indicated the presence of highly-imidized polymer on the aluminum failure surface. The XPS results indicated that failure occurred within the vapor-deposited film, very close to the aluminum/vapor-deposited-film interface. It was also evident from XPS that there was very little carboxylate formation at the locus of failure.

Sample D – PMDA/ODA Spin-coated onto Aluminum Coated with γ-APS

The elemental composition of the polymer failure surface was 76.9% carbon, 17.8% oxygen, 4.0% nitrogen, and 1.2% silicon while that of the aluminum failure surface was 50.2% carbon, 30.8% oxygen, 4.1% nitrogen, 9.9% aluminum, and 4.9% silicon. Since the aluminum failure surface contained nitrogen, aluminum, and silicon, it was clear that failure was close to the substrate surface but with some silane and polymer remaining on the surface.

High-resolution C(1s) and N(1s) XPS spectra of the polymer failure surface were similar to the spectra shown in Figures 12 and 13, respectively. The high-resolution C(1s) spectrum consisted of five peaks characteristic of a well-imidized polyimide while the N(1s) spectrum consisted of a single peak near 400.5 eV, which was also characteristic of a well-imidized polyimide.

The XPS high-resolution C(1s) and N(1s) spectra for the aluminum failure surface were also similar to the spectra shown in Figures 12 and 13, indicating that the polymer remaining on the aluminum failure surface was relatively well imidized. XPS high-resolution Al(2p) spectrum of the aluminum failure surface consisted of components due to aluminum oxide and elemental aluminum at 74.5 and 72.0 eV, respectively.

The XPS results supported the conclusion that failure was mixed, occurring mostly within the γ-APS but leaving residual clumps of polyimide on the aluminum failure surface. This conclusion was supported by results obtained from FTIR microspectroscopy. An IR

Downloaded At: 10:08 22 January 2011

microscope with a grazing angle objective lens was used to obtain reflection–absorption infrared (RAIR) spectra of several different spots on the aluminum failure surface. In some locations, the RAIR spectra were characteristic of the silane but in others the spectra were clearly characteristic of the polyimide.

DISCUSSION

First, it is clear that the adhesive fracture toughnesses that were obtained were those of interphase regions, rather than being associated with purely interfacial crack growth. This renders any comparison of the adhesive fracture energies with thermodynamic work of adhesion tenuous. The spectroscopic results indicate that the degree of imidization near the aluminum was greatest in samples *C* and *D*. These were also the samples with the highest adhesive fracture energies. In sample *C*, failure was within the vapor-deposited film, which contained very little carboxylate. In sample *D*, the locus of fracture passed through the silane coupling agent as well as regions of well-imidized polyimide. On the other hand, carboxylate formation in sample *A* inhibited proper imidization near the aluminum, which led to the formation of the most brittle interphase region of the group of controlled treatments. These observations are consistent with the fact that the adhesive fracture energies that were found here were less than the toughness of bulk polyimide. First, this was due to the incomplete imidization that was seen in sample *A* and second, even when imidization was complete, the close proximity of the stiff aluminum substrate provides constraint and should lower toughness. At the same time, the values of adhesive fracture energy that have been found are three orders of magnitude greater than the thermodynamic work of adhesion. Thus, although global plastic dissipation has been accounted for in the extraction process, other forms of dissipation must be active within the cohesive zone. These could include highly localized inelastic deformations [40].

Goldfarb and Farris [41] conducted a study where polyimide was peeled from aluminum and *vice-versa*. In addition to the usual measurements of peel force and displacement, they measured the heat flow from the specimens as they were peeled. These measurements

Downloaded At: 10:08 22 January 2011

allowed the heat flow to be subtracted from the work done to yield what was termed the internal energy change associated with fracture. The locus of fracture was the same when either the polyimide or the aluminum was peeled. While the work done in each case was of the same order, the internal energy change when the polyimide was peeled was $350\,J/m^2$ compared with $50\,J/m^2$ when the metal was peeled. This is due to the fact that, when aluminum is strained into its inelastic range, a large fraction (95%) of the work done is dissipated as heat and very little is stored. The fraction dissipated as heat drops to nearly 50% when the polymer is strained. Because the fracture characteristics were the same, regardless of which material was peeled, it was estimated that about 50 out of the $350\,J/m^2$ of internal energy of peeling the polyimide can be thought of as the adhesive fracture energy. The rest ($300\,J/m^2$) is stored in the polyimide as a high-energy structural change.

In the experiments that were conducted as part of the work described here, the processing of sample *A* (spin-coat) comes closest to that used by Goldfarb and Farris. The polyimide thickness was also quite similar. The adhesive fracture energy extracted from the cohesive zone modeling was $579\,J/m^2$, about double the internal energy of peeling that Goldfarb and Farris found. The simplest explanation for the difference is that the removal of all organic compounds *via* the plasma etching that was used here produces a cleaner aluminum surface and better bonding. Nonetheless, it is also clear that the cohesive zone models that were used here failed to differentiate between stored energy in the polyimide and the energy consumed by separation. Such an effort was beyond the scope of the analysis that was conducted here and would have to involve a coupled stress and heat transfer analysis within and without the fracture process zone.

Downloaded At: 10:08 22 January 2011

CONCLUSIONS

The adhesive fracture energies of four different polyimide/aluminum interphases were extracted from three different fracture analyses of debonding. The first two were elastic in nature, whereas the third accounted for plastic dissipation in the bulk of the peeling polyimide film and modeled the intense deformation in the fracture process zone

via a traction-separation law. The first of the elastic analyses requires the adhesive fracture energy to be obtained from measured values of pressure and central displacement. Although the ranking of adhesive fracture energies was the same, the values extracted in this way were consistently the highest. This was due to the fact that the central displacement contained a plastic component. The second elastic analysis is based on the first but only requires measured values of pressure and volume flow rate. Values of adhesive fracture energy that were obtained in this way were consistently lower but quite close to those that were obtained from the cohesive zone modeling. This was presumably due to the fact the volume flow rate is prescribed in the experiments and is, therefore, unaffected by any inelastic deformation in the peeling member. These results suggest that, if the adhesive fracture energy is required, then the approach pioneered by Chu and Durning [23] provides reasonable values in a simple manner. The cohesive zone model revealed that global plastic dissipation was 19 to 38% of the adhesive fracture energy or the energy dissipated in the process of separation.

Downloaded At: 10:08 22 January 2011

The silane treatment (*D*) gave rise to the highest value adhesive fracture energy (750 J/m^2), followed closely (700 J/m^2) by the process where the polyimide was vapor-deposited on the aluminum. XPS spectroscopic analyses revealed that the polyimide was fully imidized all the way to the aluminum in both cases. This was not so when the polyimide was spin-cast onto the aluminum surface (treatment *A*). Instead, carboxylate species were formed close to the aluminum and polymer remaining on the aluminum fracture surface was only partly imidized. As a result, the adhesive fracture energy was only 579 J/m^2.

The values of adhesive fracture energy that were determined here were all lower than that of bulk polyimide and much higher than the thermodynamic work of adhesion. The comparison with the bulk toughness is consistent with the formation of interphases that differ from the bulk (treatment *A*) and the proximity of the fracture path to the constraining aluminum substrate (treatments *C* and *D*). At the same time, the adhesive fracture energies were much higher than the thermodynamic work of adhesion. This is probably due to the fact that separation can result in highly localized deformations, which polymers store as internal energy.

Acknowledgements

The authors would like to acknowledge the partial financial support of the Office of Naval Research (N0014-95-1-1090 at UTA and N0014-93-1-0144 at UC). The use of the ABAQUS finite element code under academic license at the University of Texas at Austin is also gratefully appreciated.

References

[1] Senturia, S. D., *Polymeric Mat. Sci. Eng.* **55**, 385 (1986).
[2] Wilson, A. M., *Thin Solid Films* **83**, 145 (1981).
[3] Jensen, R. J., *Polymeric Mat. Sci. Eng.* **55**, 413 (1986).
[4] Kim, Y. H., Walker, G. F., Kim, J. and Park, J., *J. Adhes. Sci. Tech.* **1**, 331 (1987).
[5] Kim, Y. H., Walker, G. F., Feger, C. and Kowalczyk, S. P., *J. Adhes. Sci. Tech.* **2**, 95 (1988).
[6] Burrell, M. C., Codella, P. J., Fontana, J. A. and McConnell, M. D., *J. Vac. Sci. Technol.* **A7**, 55 (1989).
[7] Buchwalter, L. P., In: *Polyimides: Fundamentals and Applications*, Ghosh, M. K. and Mittal, M. K. Eds. (Marcel Dekker, New York, 1996), p. 587.
[8] Kowalczyk, S. P., Dimitrakopoulos, C. D. and Molis, S. E., *Mater. Res. Soc. Symp. Proc.* **227**, 55 (1991).
[9] Grunze, M. and Lamb, R. N., *Chem. Phys. Lett.* **133**, 283 (1987).
[10] Grunze, M. and Lamb, R. N., *Surf. Sci.* **204**, 183 (1988).
[11] Lamb, R. N., Baxter, J., Grunze, M., Kong, C. W. and Unertl, W. N., *Langmuir* **4**, 249 (1988).
[12] Strunskus, T., Grunze, M. and Gnanarajan, S., In: *Metallization of Polymers, ACS Symposium Series no. 440*, Sacher, E. S., Pireaux, J. J. and Kowalczyk, S. P. Eds. (American Chemical Society, Washington, DC, 1990).
[13] Perry, S. S. and Campion, A., *Surf. Sci. Lett.* **234**, L275 (1990).
[14] Mack, R. G., Patterson, H. H., Cook, M. R. and Carlin, C. M., *J. Polym. Sci.: Polym. Lett. Ed.* **27**, 25 (1989).
[15] Grunze, M. and Lamb, R. N., *Chem. Phys. Lett.* **133**, 283 (1987).
[16] Pethe, R. G., Carlin, C. M. and Patterson, H. H., *J. Mater. Res.* **8**, 3218 (1993).
[17] Salem, J. R., Sequeda, F. O., Duran, J., Lee, W. Y. and Yang, R. M., *J. Vac. Sci. Technol.* **A4**, 369 (1986).
[18] Buchwalter, L. P., *J. Adhesion Sci. Technol.* **4**, 697 (1990).
[19] Linde, H. and Gleason, R. T., *J. Polym. Sci., Polym. Chem. Ed.* **22**, 3043 (1984).
[20] Williams, M. L., *J. Appl. Polym. Sci.* **13**, 29 (1969).
[21] Gent, A. N. and Lewandowski, L. H., *J. Appl. Polym. Sci.* **33**, 1567 (1987).
[22] Hencky, H., *Zr. Math. Phys.* **63**, 311 (1915).
[23] Chu, Y. Z. and Durning, C. J., *J. Appl. Polym. Sci.* **45**, 1151 (1992).
[24] Chu, Y. Z., Jeong, H. S., White, R. C. and Durning, C. J., *Mat. Res. Symp. Proc.* **276**, 209 (1992).
[25] Kim, K.-S. and Aravas, N., *Int. J. Solids and Structures* **24**, 417 (1988).
[26] Kinloch, A. J., Lau, C. C. and Williams, J. G., *Int. J. Fracture* **66**, 45 (1994).
[27] Wei, Y. and Hutchinson, J. W., *J. Mech. Phys. Solids* **45**, 641 (1997).
[28] Needleman, A., *J. Appl. Mech.* **54**, 525 (1987).
[29] Needleman, A., *J. Mech. Phys. Solids* **38**, 289 (1990).
[30] Tvergaard, V. and Hutchinson, J. W., *J. Mech. Phys. Solids* **41**, 1119 (1993).

Downloaded At: 10:08 22 January 2011

[31] Tvergaard, V. and Hutchinson, J. W., *Int. J. Solids and Structures* **31**, 823 (1994).
[32] Swadener, J. G. and Liechti, K. M., *J. Appl. Mech.* **65**, 25 (1998).
[33] Liechti, K. M. and Chai, Y.-S., *J. Appl. Mech.* **59**, 295 (1992).
[34] Shirani, A. and Liechti, K. M., *Int. J. Fracture* **93**, 281 (1998).
[35] McCrackin, F. L. and Colson, J., *Natl. Bur. Stds. Tech. Note 242* (U.S. Govt. Print. Off., Washington, DC, 1964).
[36] Shirani, A., *Ph.D. Dissertation*, Engineering Mechanics Research Laboratory Report, EMRL 97-16, The University of Texas at Austin (1997).
[37] Paek, B.-H. and Durning, C. J., *J. Adhesion* **68**, 269 (1998).
[38] Liechti, K. M. and Shirani, A., *Int. J. Fracture* **67**, 21 (1994).
[39] Buchwalter, P. L. and Baise, A. I., In: *Polyimides: Synthesis, Characterization, and Applications*, Vol. 1, Mittal, K. L. Ed. (Plenum Press, New York, 1984), p. 537.
[40] Swadener, J. G., Liechti, K. M. and de Lozanne, A. L., *J. Mech. Phys. Solids* **47**, 223 (1999).
[41] Goldfarb, J. L. and Farris, R. J., *J. Adhesion* **35**, 233 (1991).

Downloaded At: 10:08 22 January 2011